

# Reconstruction algorithms for photoacoustic tomography in heterogenous damping media

Linh V. Nguyen

Department of Mathematics, University of Idaho  
875 Perimeter Dr, Moscow, ID 83844, USA  
lnguyen@uidaho.edu

Markus Haltmeier

Department of Mathematics, University of Innsbruck  
Technikerstrasse 13, 6020 Innsbruck, Austria  
markus.haltmeier@uibk.ac.at

August 19, 2018

## Abstract

In this article, we study several reconstruction methods for the inverse source problem of photoacoustic tomography (PAT) with spatially variable sound speed and damping. The backbone of these methods is the adjoint operators, which we thoroughly analyze in both the  $L^2$ - and  $H^1$ -settings. They are casted in the form of a nonstandard wave equation. We derive the well-posedness of the aforementioned wave equation in a natural functional space, and also prove the finite speed of propagation. Under the uniqueness and visibility condition, our formulations of the standard iterative reconstruction methods, such as Landweber's and conjugate gradients (CG), achieve a linear rate of convergence in either  $L^2$ - or  $H^1$ -norm. When the visibility condition is not satisfied, the problem is severely ill-posed and one must apply a regularization technique to stabilize the solutions. To that end, we study two classes of regularization methods: (i) iterative, and (ii) variational regularization. In the case of full data, our simulations show that the CG method works best; it is very fast and robust. In the ill-posed case, the CG method behaves unstably. Total variation regularization method (TV), in this case, significantly improves the reconstruction quality.

**Keywords:** Photoacoustic tomography, Tikhonov regularization, total variation, attenuation, visibility condition, adjoint operator, finite speed of propagation.

## 1 Introduction

Photoacoustic tomography (PAT) is an emerging hybrid method of imaging that combines the high contrast of optical imaging with the good resolution of ultrasound

tomography. As illustrated in Figure 1, the biological object of interest is scanned with a pulsed optical illumination. The photoelastic effect causes a thermal expansion and a subsequent ultrasonic wave propagating in space. One measures the ultrasonic pressure on an observation surface outside of the object. The aim of PAT is to recover the initial pressure distribution inside the tissue from the measured data. The initial pressure distribution contains helpful internal information of the object and is the image to be reconstructed.

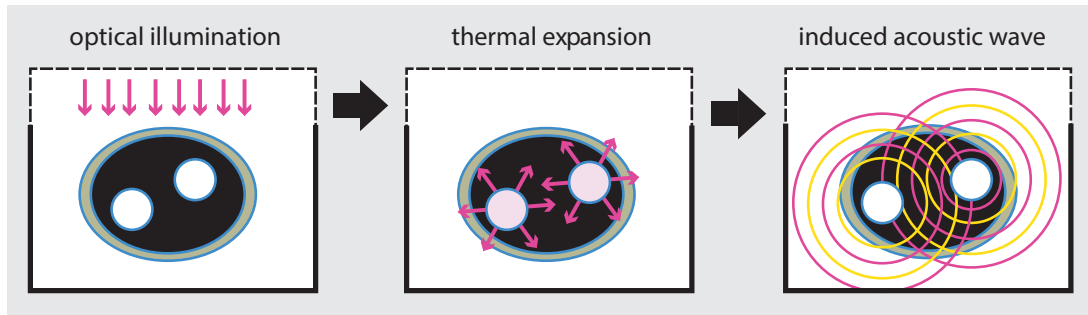


Figure 1: Left: A biological object is illuminated with an optical pulse. Middle: Absorption of optical energy causes thermal expansion. Right: Thermal expansion induces an ultrasonic wave that is measured outside of the sample and used to reconstruct the image of the object.

The standard model in PAT assumes homogeneous non-damping acoustic media and has been well studied. There exist several methods to solve the corresponding inverse problem of PAT such as explicit inversion formulas [18, 58, 34, 17, 39, 20, 21, 38, 43], series solutions [35, 2], time reversal [18, 26, 25, 50, 51], and quasi-reversibility [12]. Reviews on these methods can be found in [26, 32, 33, 46]. Discrete iterative approaches, which are based on a discretization of the forward problem together with numerical solution methods for solving the resulting system of linear equations can be found in [45, 44, 59, 15, 57, 47, 27, 56]. Recently, iterative schemes in a Hilbert space settings have also been introduced and studied; see [6, 8, 22].

**PAT in heterogenous damping media:** In this article, we are interested in PAT accounting for spatially variable sound speed and spatially variable damping. It is still an ongoing research which is the correct model for attenuation, and several different modeling equations have been used (see, for example, [36, 37, 4, 31, 1, 3, 9, 24, 30, 42, 55]). For mathematical interest, we consider a simple attenuation model using the damped wave equation, which reads

$$\begin{aligned}
 [c^{-2}(x) \partial_{tt} + a(x) \partial_t - \Delta]p(x, t) &= 0 && \text{on } \mathbb{R}^d \times \mathbb{R}_+, \\
 p(x, 0) &= f(x) && \text{on } \mathbb{R}^d, \\
 p_t(x, 0) &= -c^2(x) a(x) f(x) && \text{on } \mathbb{R}^d.
 \end{aligned} \tag{1}$$

Here,  $c: \mathbb{R}^d \rightarrow \mathbb{R}$  is the variable sound speed,  $a: \mathbb{R}^d \rightarrow \mathbb{R}$  the variable damping coefficient, and  $f: \mathbb{R}^d \rightarrow \mathbb{R}$  the desired initial pressure. We assume that  $c$  and  $a$  are smooth functions,  $c$  is bounded between two positive constants, and  $a \geq 0$ . Let us denote by

$S$  the observation surface and by  $T > 0$  the final measurement time. We will assume that  $S$  is a (relatively) closed subset of  $\partial\Omega$  with nonempty interior  $\text{Int}(S)$ , where  $\Omega$  is an open subset of  $\mathbb{R}^d$  that contains the support of  $f$ . The mathematical problem of PAT is to invert the map  $\mathbf{W}: f \mapsto g := p|_{S \times (0, T)}$ . It is referred to as the inverse source problem of PAT. In this article, we assume that  $\mathbf{W}$  is injective (that is, the reconstruction is unique). For the full data problem, it holds as long as  $T > \max_{x \in \Omega} \text{dist}(x, \partial\Omega)$  (see, [1]). The injectivity of  $\mathbf{W}$  in the case of partial data is still an open problem and beyond the scope of this article.

There are only few papers analyzing the damped wave equation (1) for PAT [24, 42, 1]. In [24], some interesting microlocal analysis results have been derived for (1) and a time-reversal framework for image reconstruction has been proposed. This time reversal method is only proved to converge (linearly) to the exact solution when the attenuation coefficient is small enough. In the recent work [42] a modification of the time reversal method has been proposed that converges (linearly) to the solution for arbitrarily large attenuation coefficient. A more general model was considered in [1]. Let us mention that, in order for the algorithm to converge, both papers assume that the data is measured on a closed surface completely surrounding the object (i.e., full data problem). Opposed to that, the analysis and algorithms we derive in the present paper apply to the partial data problem as well as the full data problem.

**Main contributions:** In this article, we establish the mathematical foundation of several reconstruction methods for the inverse source problem of PAT with variable sound speed and damping. Namely, we formulate the adjoint operator in the continuous setting using a nonstandard wave equation. We prove the well-posedness of the adjoint equation in a natural setting and its finite speed of propagation. We then propose and analyze various iterative reconstruction algorithms for PAT employing our knowledge of the adjoint operator. We study both the full and limited data cases. Under the uniqueness and the visibility condition (described in Section 3.1), our algorithms converge linearly to the solution, even for the partial data problem. The convergence is shown in the  $L^2$ -type norm (on image and pre-image space) and the  $H^1$ -type norm. We note that convergences in the  $H^1$ -type norm have been a common practice in the inverse source problem of PAT (see for example [24, 42]). However, in practice, the image to be recovered may not be in  $H^1$ . Therefore, having convergence in the  $L^2$ -norm is helpful, too.

In case that the visibility condition does not hold, the inverse problem of PAT is severely ill-posed and regularization methods have to be applied for its solution. For that purpose Landweber's, the steepest descent and the CG method can be applied as well, since they are known to be regularization methods when combined with Morozov's discrepancy principle [16, 23, 29]. Additionally, we study generalized Tikhonov regularization [48], which consists in minimizing the penalized residual functional  $\Phi(f) = \frac{1}{2} \|\mathbf{W}f - g\|^2 + \lambda \mathbf{G}(f)$ . Here  $\mathbf{G}: \mathcal{X} \rightarrow [0, \infty]$  is a convex regularization term and  $\lambda > 0$  is the regularization parameter. In particular, we investigate the quadratic,  $\mathbf{G}(f) = \int_{\Omega} |\nabla f|^2$ , and the total variation (TV),  $\mathbf{G}(f) = \int_{\Omega} |\nabla f|$ , regularizations. In the quadratic case, the above iterative methods can again be applied to minimize  $\Phi$ . For the latter case, we use the minimization algorithm of [49], which is a special instance of the Chambolle-Pock algorithm [11]. Using a discretization of the forward operator

with matched discrete adjoint, variational methods including TV minimization have been applied in [27]. Using continuous formulations of the adjoint, variational methods have been applied to PAT in [5, 28]. Our application of variational regularization for the damped wave equation (1) is new.

**Outline:** The article is organized as follows. In Section 2, we derive the explicit formulation of the adjoint operator. We also discuss some properties of the adjoint equation. In Section 3, we study the inverse problem of PAT in inhomogeneous damping media. We show that the inverse problem of PAT is well-posed under the visibility condition (see Subsection 3.1). We analyze iterative and variational reconstruction algorithms in the well-posed and the ill-posed cases. In section 4, we present various numerical examples for the proposed methods. The main theoretical result, the analysis of the adjoint equation, is presented Appendix A.1. We briefly describe the  $k$ -wave method, which we use for our forward and adjoint simulation, in Appendix A.2.

## 2 The adjoint operator for PAT

Let us recall that the PAT forward operator is given by  $\mathbf{W}: f \mapsto g := p|_{S \times (0, T)}$ , where  $p$  is defined by the acoustic wave equation (1) and  $S$  is a closed subset of  $\partial\Omega$ . Our goal is to invert  $\mathbf{W}$  using the methods introduced in the following section. It is crucial to analyze the adjoint operator  $\mathbf{W}^*$  of  $\mathbf{W}$ . To that end, we first need to identify the correct mapping spaces for  $\mathbf{W}$ . We, indeed, will consider two realizations,  $\mathbf{W}_0$  and  $\mathbf{W}_1$ , of  $\mathbf{W}$  corresponding to two different choices of the mapping spaces.

We first assume that  $\text{supp}(f) \subset \Omega_0$ , where  $\Omega_0 \Subset \Omega$ . For the spaces of  $f$ , let us denote

$$\begin{aligned}\mathcal{X}_0 &:= \{f \in L^2(\mathbb{R}^d) : \text{supp}(f) \subset \overline{\Omega}_0\}, \\ \mathcal{X}_1 &:= \{f \in H^1(\mathbb{R}^d) : \text{supp}(f) \subset \overline{\Omega}_0\}.\end{aligned}$$

Then,  $\mathcal{X}_0$  and  $\mathcal{X}_1$  are Hilbert spaces with the respective norms  $\|f\|_{\mathcal{X}_0} = \|c^{-1}f\|_{L^2(\Omega_0)}$  and  $\|f\|_{\mathcal{X}_1} = \|\nabla f\|_{L^2(\Omega_0)}$ . We note that  $\mathcal{X}_0 \cong L^2(\Omega_0)$  and  $\mathcal{X}_1 \cong H_0^1(\Omega_0)$ . The above chosen norms are convenient for our later purposes.

For the spaces of  $g$ , we fix a nonnegative function  $\chi \in C^\infty(\partial\Omega \times [0, T])$  such that  $\text{supp}(\chi) = \Gamma := S \times [0, T]$ . Let us denote:

$$\begin{aligned}\mathcal{Y}_0 &= \{g : \|g\|_{\mathcal{Y}_0} := \|\sqrt{\chi}g\|_{L^2(\Gamma)} < \infty\}, \\ \mathcal{Y}_1 &= \{g : g(\cdot, 0) \equiv 0, \|g\|_{\mathcal{Y}_1} := \|g_t\|_{\mathcal{Y}_0} < \infty\}.\end{aligned}$$

We define

$$\mathbf{W}_i = \mathbf{W}|_{\mathcal{X}_i} : (\mathcal{X}_i, \|\cdot\|_{\mathcal{X}_i}) \rightarrow (\mathcal{Y}_i, \|\cdot\|_{\mathcal{Y}_i}) \quad \text{for } i = 0, 1.$$

Let  $H^i(\Gamma)$  be the standard Sobolev space of order  $i$  on  $\Gamma$ . Notice that  $\mathbf{W}$  is a bounded map from  $\mathcal{X}_i \rightarrow H^i(\Gamma)$ . This comes from the fact that  $\mathbf{W}$  is the sum of two Fourier integral operators of order zero (see, e.g., [24, Lemma 3]). Since  $H^i(\Gamma) \subset \mathcal{Y}_i$ , we obtain:

**Theorem 1.** *For  $i = 0, 1$ ,  $\mathbf{W}_i$  is a bounded map from  $\mathcal{X}_i$  to  $\mathcal{Y}_i$ .*

From now on, we consider  $\chi g$  as a function on  $\partial\Omega \times [0, T]$ , which vanishes on  $(\partial\Omega \setminus S) \times [0, T]$ . The following theorem gives us an explicit formulation of the adjoint operator  $\mathbf{W}_i^*$  of  $\mathbf{W}_i$ :

**Theorem 2.** *The following results hold.*

(a) *Let  $g \in H^1([0, T]; H^{-1/2}(\partial\Omega)) \cap \mathcal{X}_0$ . Consider the wave equation*

$$\begin{aligned} [c^{-2} \partial_{tt} - a \partial_t - \Delta]q &= 0, \quad (\mathbb{R}^d \setminus \partial\Omega) \times (0, T), \\ q(T) &= 0, \quad q_t(T) = 0, \\ [q] &= 0, \quad \left[ \frac{\partial q}{\partial \nu} \right] = \chi g. \end{aligned} \tag{2}$$

Here,  $[q]$  denote the jump of  $q$  across the boundary  $\partial\Omega$ . Then

$$\mathbf{W}_0^* g = q_t(0)|_{\Omega_0}.$$

(b) *Let  $g \in H^1([0, T]; H^{-1/2}(\partial\Omega)) \cap \mathcal{X}_1$ . Assume further that  $\chi$  is independent of  $t$  (i.e.,  $\chi(y, t) = \chi(y)$ ). We define*

$$\bar{g}(x, t) = g(x, t) - g(x, T),$$

and consider the wave equation

$$\begin{aligned} [c^{-2} \partial_{tt} - a \partial_t - \Delta]\bar{q} &= 0, \quad (\mathbb{R}^d \setminus \partial\Omega) \times (0, T), \\ \bar{q}(T) &= 0, \quad \bar{q}_t(T) = 0, \\ [\bar{q}] &= 0, \quad \left[ \frac{\partial \bar{q}}{\partial \nu} \right] = \chi \bar{g}. \end{aligned} \tag{3}$$

Then,

$$\mathbf{W}_1^* g = \Pi[\bar{q}_t(0)].$$

Here,  $\Pi$  is the projection on the space  $\mathcal{X}_1 \cong H_0^1(\Omega_0)$ , given by

$$\Pi(f) = f - \phi,$$

where  $\phi$  is the harmonic extension of  $f|_{\partial\Omega_0}$  to  $\bar{\Omega}_0$ .

The proof for Theorem 2 is similar to that of [22, Theorem 3.2]. We skip it for the sake of brevity. The analysis of (2), which is the main theoretical achievement of this article, is presented in Theorem 8. Namely, we show that if  $g \in H^1([0, T]; H^{-1/2}(\partial\Omega))$ , equation (2) has a unique solution  $q \in L^2([0, T]; H^1(\mathbb{R}^d))$  satisfying  $q' \in L^2([0, T]; L^2(\mathbb{R}^d))$ , and  $q'' \in L^2([0, T]; H^{-1}(\mathbb{R}^d))$ . Moreover,  $q$  satisfies the finite speed of propagation: let  $c_+ = \max_{x \in \mathbb{R}^d} c(x)$ , then  $q(x, t) = 0$  for any  $(x, t) \in \Omega^c \in [0, T]$  such that  $\text{dist}(x, \partial\Omega) \geq c_+(T - t)$ . In the absence of damping (i.e.,  $a = 0$ ), an existence and uniqueness of equation (2) has been proved in [8]. Compared to their result, we require less regularity on  $g$  and the solution space is more natural. Moreover, the finite speed of propagation is new. It helps us to truncate the calculation domain when needed.

**Remark 3.** *Let us make the following observations:*

- (a) Since  $H^1([0, T]; H^{-1/2}(\partial\Omega)) \cap \mathcal{Y}_i$  is dense in both  $\mathcal{Y}_i$  for  $i = 0, 1$ , the adjoint operators  $\mathbf{W}_0^*$  and  $\mathbf{W}_1^*$  are uniquely determined from the formulas in Theorem 2.
- (b) Compared to  $\mathbf{W}_0^*$ ,  $\mathbf{W}_1^*$  involves an extra projection operator. In our numerical experiments, we will only use  $\mathbf{W}_0^*$  since it is simpler to implement. However, the knowledge of  $\mathbf{W}_1^*$  is helpful in designing iterative algorithms that converge in the  $H^1$ -norm.

### 3 Solution to the inverse problem

In this section, we present methods for inverting the two realizations  $\mathbf{W}_i: \mathcal{X}_i \rightarrow \mathcal{Y}_i$  for  $i = 0, 1$ . To that end, we first show that the inverse problems are well posed under the visibility condition. We then separately consider the well-posed and ill-posed situation.

#### 3.1 Well-posedness under the visibility condition

Let us fix several geometric conventions. We will always assume that the sound speed  $c$  is smooth and bounded from below by a positive constant. The space  $\mathbb{R}^d$  is considered as a Riemannian manifold with the metric  $c^{-2}(x) dx^2$  and  $\Omega$  is assumed to be strictly convex with respect to this metric. Then, all the geodesic rays originating inside  $\Omega$  intersect the boundary  $\partial\Omega$  at most once. We also assume that the speed  $c$  is nontrapping, i.e., all such geodesic rays intersect with  $\partial\Omega$ . Also,  $\mathcal{T}^*\Omega \setminus 0$  is the cotangent bundle of  $\Omega$  minus the zero section, which can be identified with  $\Omega \times (\mathbb{R}^d \setminus \{0\})$ .

**Visibility condition:** *There is a closed subset  $S_0 \subset \partial\Omega$  such that  $S_0 \subset \text{Int}(S)$  and the following condition holds: for any element  $(x, \xi) \in \mathcal{T}^*\Omega_0 \setminus 0$ , one of the unit speed geodesic rays originating from  $x$  at time  $t = 0$  along the directions  $\pm\xi$  intersects transversally with  $S_0$ , at a time  $t < T$ .*

Let us recall that, in this article, we will always assume the injectivity of  $\mathbf{W}_i$ . Our first result is that the inversion of  $\mathbf{W}_i$  is stable under the visibility condition.

**Theorem 4.** *Assume that the visible condition holds and  $\chi \equiv 1$  on  $S_1 \times [0, T]$ , where  $S_1$  is a closed subset of  $\partial\Omega$  such that  $S_0 \subset \text{Int}(S_1)$  and  $S_1 \subset \text{Int}(S)$ . For  $i = 0, 1$ , there is a constant  $C > 0$  such that for any  $f \in \mathcal{X}_i$ , we have*

$$\|f\|_{\mathcal{X}_i} \leq C \|g\|_{\mathcal{Y}_i} \quad \text{where } g = \mathbf{W}f. \quad (4)$$

One proof virtually follows from [22, Theorem 3.4] line by line. One only needs to refer to [24] instead of [50] when needed. We briefly present here another approach.

*Proof.* Observe that  $\mathbf{W}_i^* \mathbf{W}_i$  is, similarly to the non-damping case (see [22, Theorem 3.6]), an elliptic operator from  $\mathcal{X}_i$  into itself with the principal symbol  $\sigma(x, \xi)$  being bounded from below by a positive constant  $\delta$ . We then have

$$\|\mathbf{W}_i f\|_{\mathcal{Y}_i}^2 = \langle \mathbf{W}_i^* \mathbf{W}_i f, f \rangle_{\mathcal{X}_i} \geq \delta \langle f, f \rangle_{\mathcal{X}_i} + \langle \mathbf{K}f, f \rangle_{\mathcal{X}_i},$$

where  $\mathbf{K}$  is a compact operator. Young's inequality gives

$$\|f\|_{\mathcal{X}_i}^2 \leq C(\|\mathbf{W}_i f\|_{\mathcal{Y}_i}^2 + \|\mathbf{K}f\|_{\mathcal{X}_i}).$$

The injectivity of  $\mathbf{W}_i$  and [53, Theorem V.3.1] gives

$$\|f\|_{\mathcal{X}_i}^2 \leq C\|\mathbf{W}_i f\|_{\mathcal{Y}_i}^2. \quad \square$$

---

**Algorithm 1** Steepest descent method for  $\mathbf{W}_i f = g^\delta$ .

---

- 1: Initialize  $f_0^\delta = 0$ ;  $k \leftarrow 0$
  - 2: **while** stopping criteria not satisfied **do**
  - 3:    $s_k = \mathbf{W}_i^*(\mathbf{W}_i f_k^\delta - g^\delta)$
  - 4:    $\gamma_k = \|s_k\|_{\mathcal{X}_i}^2 / \|\mathbf{W}_i s_k\|_{\mathcal{Y}_i}^2$
  - 5:    $f_{k+1}^\delta = f_k^\delta - \gamma_k s_k$
  - 6:    $k \leftarrow k + 1$
  - 7: **end while**
- 

---

**Algorithm 2** CGNE method for  $\mathbf{W}_i f = g^\delta$ .

---

- 1: Initialize  $f_0^\delta = 0$ ;  $r_0 = g^\delta - \mathbf{W}_i f_0^\delta$ ;  $d_0 = \mathbf{W}_i^* r_0$ ;  $k \leftarrow 0$
  - 2: **while** stopping criteria not satisfied **do**
  - 3:    $\alpha_k = \|\mathbf{W}_i^* r_k\|_{\mathcal{X}_i}^2 / \|\mathbf{W}_i d_k\|_{\mathcal{Y}_i}^2$
  - 4:    $f_{k+1}^\delta = f_k^\delta + \alpha_k d_k$
  - 5:    $r_{k+1} = r_k - \alpha_k \mathbf{W}_i d_k$
  - 6:    $\beta_k = \|\mathbf{W}_i^* r_{k+1}\|_{\mathcal{X}_i}^2 / \|\mathbf{W}_i^* r_k\|_{\mathcal{X}_i}^2$
  - 7:    $d_{k+1} = \mathbf{W}_i^* r_{k+1} + \beta_k d_k$
  - 8:    $k \leftarrow k + 1$
  - 9: **end while**
- 

### 3.2 Well posed case: Linear convergence of iterative methods

When the linear inverse problem  $\mathbf{W}f = g$  is well-posed, then Landweber's, the steepest descent, and the CG methods applied to  $g^\delta$  converge to a minimizer of

$$\Phi_0: \mathcal{X}_i \rightarrow \mathbb{R}: f \mapsto \frac{1}{2}\|\mathbf{W}_i f - g^\delta\|_{\mathcal{Y}_i}^2 \quad (5)$$

with a linear rate of convergence (for both realizations  $\mathbf{W}_i: \mathcal{X}_i \rightarrow \mathcal{Y}_i$  of  $\mathbf{W}$ ). Here, we assume that  $f \in \text{Dom}(\mathbf{W}_i)$  and  $g^\delta \in \mathcal{Y}_i$  is such that  $\|\mathbf{W}_i f - g^\delta\|_{\mathcal{Y}_i} < \delta$ . For convenience of the reader the steepest descent and the CG iteration are recalled in Algorithms 1 & 2. The Landweber's method is the same as the steepest descent method with the modification that the step size  $\gamma_k$  is replaced by a constant value  $\gamma$  satisfying  $0 < \gamma < 2/\|\mathbf{W}_i^* \mathbf{W}_i\|$ . Theorem 4 implies the following result.

**Theorem 5.** *Assume that the visible condition holds and let  $\chi \equiv 1$  on  $S_1 \times [0, T]$ , where  $S_1$  is a closed subset of  $\partial\Omega$  such that  $S_0 \subset \text{Int}(S_1)$  and  $S_1 \subset \text{Int}(S)$ .*

- For any  $g^\delta \in \mathcal{Y}_i$ , the Landweber, the steepest descent and the CG iteration converge linearly to the unique minimizer  $f^\delta$  of (5). More precisely, there is a constant  $a < 1$  (only depending on the realization and the iterative method) such that the iterates  $f_k^\delta$  defined by either method satisfy  $\|f^\delta - f_k^\delta\|_{\mathcal{X}_i} \leq a^k \|f^\delta\|_{\mathcal{X}_i}$  for  $k \in \mathbb{N}$ .
- For  $\delta = 0$ , the limit  $f^0$  is the unique solution of  $\mathbf{W}_i f = g$ . Moreover, we have  $\|f - f^\delta\|_{\mathcal{X}_i} \leq C\delta$ , where  $C$  is the constant appearing in Theorem 4.

*Proof.* Theorem 4 shows that the inverse problem is well-posed. The above results follow directly from the standard theory of iterative methods [23, 16, 29].  $\square$

Theorem 5 shows that with our choices of mapping spaces, the Landweber's, steepest descent, and CG methods converge linearly in the  $L^2$ -norm as well as the  $H^1$ -norm.

### 3.3 Ill-posed case: regularization

Now consider the situation where the visibility condition does not hold. Then one has to apply regularization methods.

**Iterative regularization methods:** We consider the Landweber, the steepest descent and the CG methods combined with Morozov's discrepancy principle. According to the discrepancy principle, the iteration is terminated at the index

$$k(\delta, g^\delta) = \arg \min \left\{ k \in \mathbb{N} : \|\mathbf{W}_i f_{k+1}^\delta - g^\delta\|_{\mathcal{X}_i} \leq \tau\delta \right\}$$

with some fixed  $\tau > 1$ .

**Theorem 6.** *Suppose  $f \in \mathcal{X}_i$ ,  $\delta > 0$ , let  $g^\delta \in \mathcal{Y}_i$  satisfy  $\|g^\delta - \mathbf{W}f\|_{\mathcal{Y}_i} \leq \delta$  and define  $(f_k^\delta)_{k \in \mathbb{N}}$  by either the Landweber, steepest descent or the CG iteration.*

1. Exact data: If  $\delta = 0$ , then  $\|f_k - f\|_{\mathcal{X}_i} \rightarrow 0$  as  $k \rightarrow \infty$ .
2. Noisy data: Let  $(\delta(m))_{m \in \mathbb{N}} \in (0, \infty)^\mathbb{N}$  converge to zero and let  $(g_m)_{m \in \mathbb{N}} \in \mathcal{Y}_i$  satisfy  $\|g_m - \mathbf{W}f\|_{\mathcal{Y}_i} \leq \delta(m)$ . Then the following hold:
  - The stopping indices  $k_*(\delta(m), g_m)$  are well defined;
  - We have  $\|f_{k_*(\delta(m), g_m)}^{\delta(m)} - f\|_{\mathcal{X}_i} \rightarrow 0$  as  $m \rightarrow \infty$ .

*Proof.* The claims follow from standard results for iterative regularization methods (see, for example, [23, 16, 29]).  $\square$



**Variational (penalized) regularization methods:** As an alternative to iterative regularization methods we will apply generalized Tikhonov regularization, which has the advantage that a-priori information can be more easily explicitly incorporated. In this work we apply  $H^1$ -regularization and TV-regularization,

$$\Phi_2(f) := \frac{1}{2} \|\mathbf{W}f - g\|_{\mathcal{Y}_0}^2 + \frac{\lambda}{2} \int_{\Omega_0} |\nabla f|^2, \quad (6)$$

$$\Phi_1(f) := \frac{1}{2} \|\mathbf{W}f - g\|_{\mathcal{Y}_0}^2 + \lambda \int_{\Omega_0} |\nabla f|, \quad (7)$$

respectively. Here  $\lambda > 0$  is the regularization parameter and both functionals are considered as mappings on  $\mathcal{X}_0 = L^2(\Omega_0)$ . From the general theory of variational regularization methods, it follows that (6) and (7) again yield regularization methods [48].

For numerically minimizing the Tikhonov functionals (6) and (7), we replace them by the discrete counterparts

$$\Phi_2(\mathbf{f}) := \frac{1}{2} \|\mathbf{W}\mathbf{f} - \mathbf{g}^\delta\|_2^2 + \frac{\lambda}{2} \|\mathbf{D}\mathbf{f}\|_2^2, \quad (8)$$

$$\Phi_1(\mathbf{f}) := \frac{1}{2} \|\mathbf{W}\mathbf{f} - \mathbf{g}^\delta\|_2^2 + \lambda \|\mathbf{D}\mathbf{f}\|_1. \quad (9)$$

Here  $\mathbf{f} \in \mathbb{R}^N$ ,  $\mathbf{g}^\delta \in \mathbb{R}^M$ ,  $\mathbf{W}: \mathbb{R}^N \rightarrow \mathbb{R}^M$  is the discretization of the forward operator and  $\mathbf{D}: \mathbb{R}^N \rightarrow \mathbb{R}^N \times \mathbb{R}^N$  denotes the discrete gradient. The functional (8) is quadratic and can be minimized, for example, with the steepest descent or the CG iteration. The discrete TV problem (9) can also be minimized by various methods. In this work we use the minimization algorithm of [49], which is a special instance of the Chambolle-Pock algorithm [11] and summarized in Algorithm 3.

---

**Algorithm 3** Algorithm for minimizing (9)

---

- 1:  $L \leftarrow \|(\mathbf{W}, \mathbf{D})\|_2$ ;  $\tau := 1/L$ ;  $\sigma := 1/L$ ;  $\theta := 1$ ;  $k \leftarrow 0$
  - 2: initialize  $\mathbf{f}_0$ ,  $\mathbf{p}_0$ , and  $\mathbf{q}_0$  to zero values
  - 3:  $\mathbf{u}_0 \leftarrow \mathbf{f}_0$
  - 4: **while** stopping criteria not satisfied **do**
  - 5:    $\mathbf{p}_{k+1} \leftarrow (\mathbf{p}_k + \sigma(\mathbf{W}\mathbf{u}_k - \mathbf{g}^\delta))/(1 + \sigma)$
  - 6:    $\mathbf{q}_{k+1} \leftarrow \lambda(\mathbf{q}_k + \sigma\mathbf{D}\mathbf{u}_k) / \max\{\lambda\mathbf{1}, |\mathbf{q}_k + \sigma\mathbf{D}\mathbf{u}_k|\}$
  - 7:    $\mathbf{f}_{k+1} \leftarrow \mathbf{f}_k - \tau\mathbf{W}^\top\mathbf{p}_{k+1} + \tau\mathbf{D}^\top\mathbf{q}_{k+1}$
  - 8:    $\mathbf{u}_{k+1} \leftarrow \mathbf{f}_{k+1} + \theta(\mathbf{f}_{k+1} - \mathbf{f}_k)$
  - 9:    $k \leftarrow k + 1$
  - 10: **end while**
- 

## 4 Numerical examples

In this section we present numerical examples for full data (well-posed case) as well as for limited view data (ill-posed case). For both cases we take  $\Omega = [-1, 1]^2$  and  $\Omega_0 = B_{0.9}(0)$ , the ball with radius 0.9 centered at the origin. We also assume variable sound speed and variable attenuation profile. We consider the realization of the

operator  $\mathbf{W} = \mathbf{W}_0: \mathcal{X}_0 \rightarrow \mathcal{Y}_0$  using the  $L^2$ -norm. For the forward and the adjoint equations, the wave equation is solved with a variant of the  $k$ -space method that is described in Appendix A.2. The  $k$ -pace method yields solutions that are periodic with period determined by the size of the computational domain. To avoid effects of periodization in all numerical simulations the domain  $\Omega = [-1, 1]^2$  is embedded in a larger computational domain  $[-2, 2]^2$ .

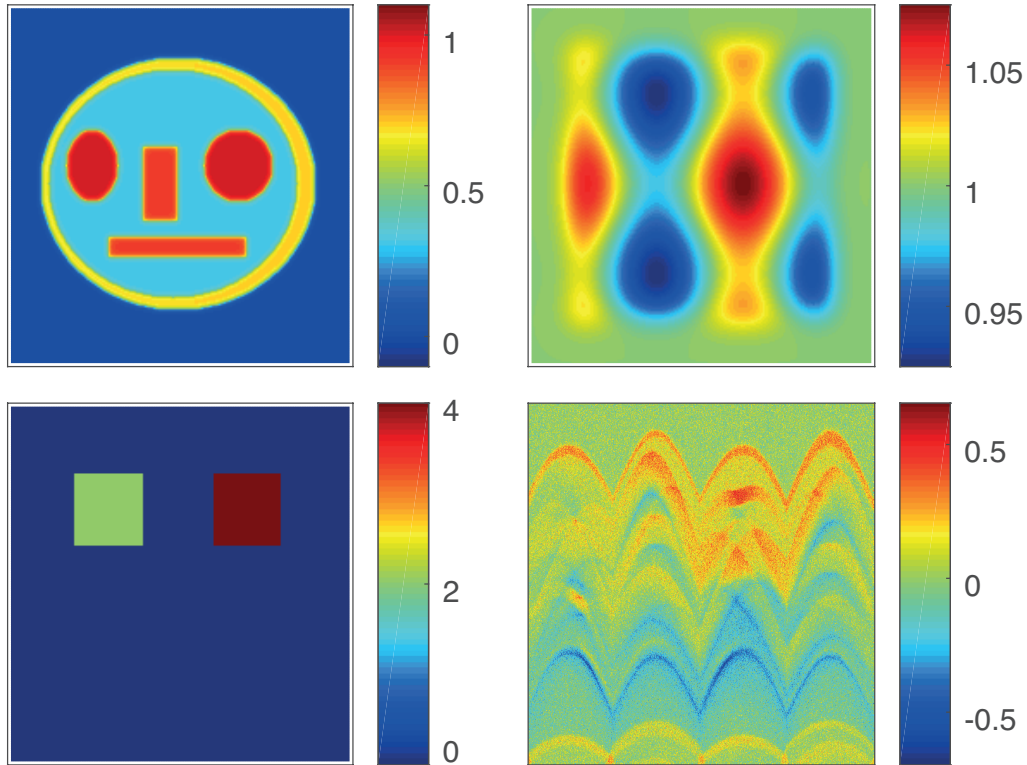


Figure 2: Phantom (top left), variable sound speed (top right), variable attenuation coefficient (bottom left) and data with added noise (bottom right).

The initial phantom, the sound speed and the attenuation are shown in Figure 2. All these functions are represented by discrete vectors in  $\mathbb{R}^{201 \times 201}$ . The computed data  $g \in \mathbb{R}^{800 \times 501}$  corresponds to discrete pressure values at the 800 boundary pixels on  $\partial\Omega$  and 501 equidistant time samples in  $[0, 2.5]$ . The (full data) discrete forward operator  $W: \mathbb{R}^{201 \times 201} \rightarrow \mathbb{R}^{800 \times 501}$  is obtained by restricting the numerical solution to the boundary pixels. The discretization  $W^T: \mathbb{R}^{800 \times 501} \rightarrow \mathbb{R}^{201 \times 201}$  of the adjoint operator is also computed using the  $k$ -space method. In order to avoid inverse crime, in all simulations we use a twice finer discretization for the data simulation than for the reconstruction (followed by restriction to the  $800 \times 501$  grid).

#### 4.1 Full view data (well-posed case)

We first study the well-posed case where the data is given on the whole boundary. The standard iterative methods (Landweber, steepest descent and CG) are therefore

linearly convergent.

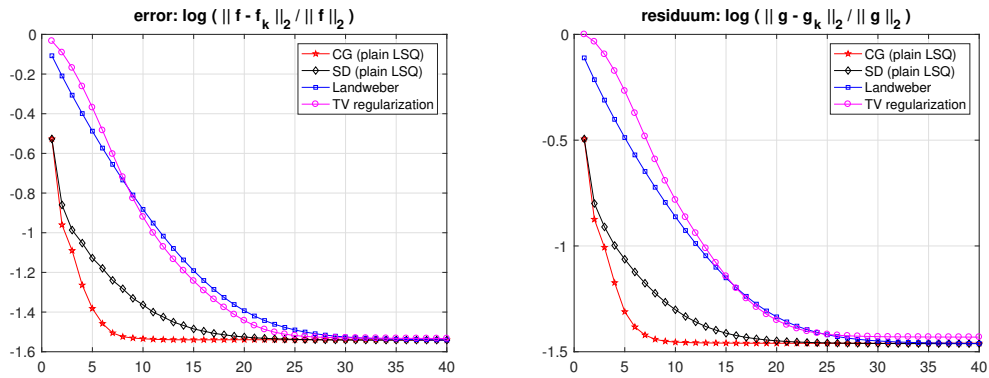


Figure 3: Errors and residuals for the full data case without added noise.

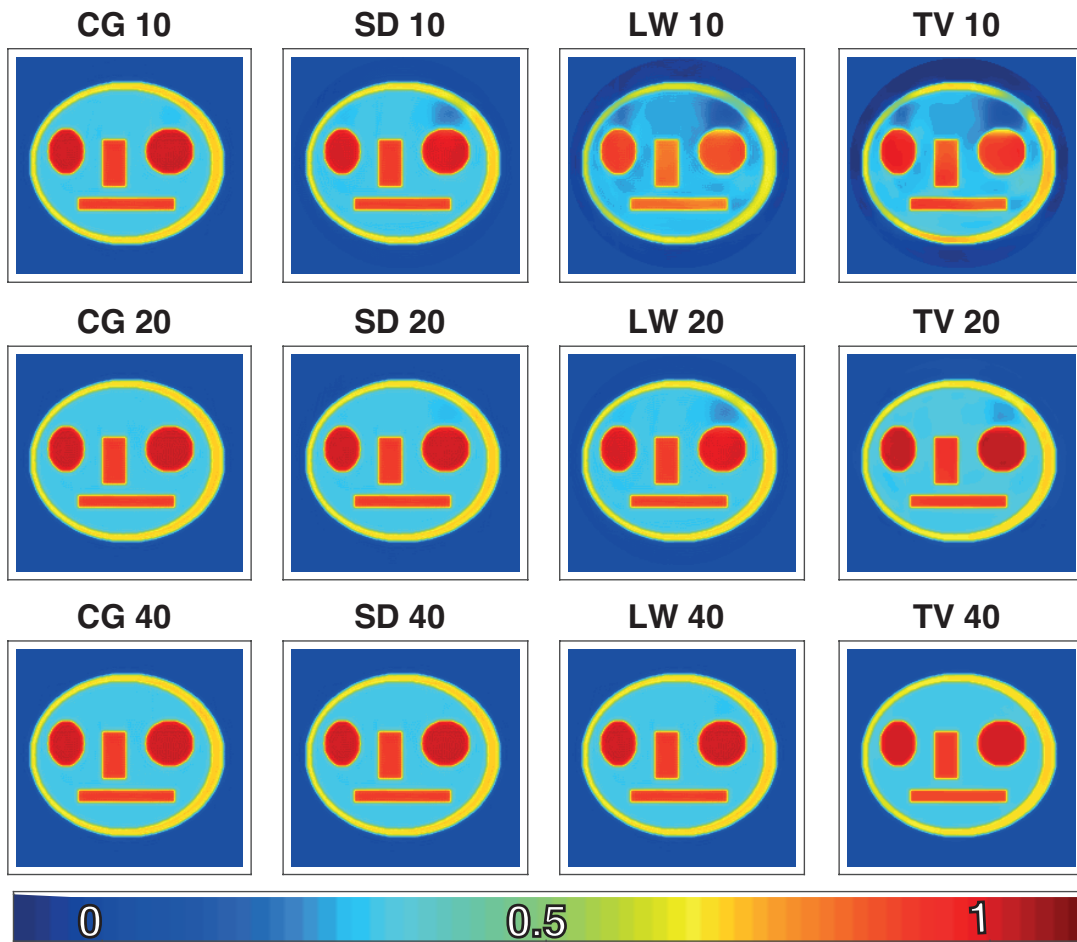


Figure 4: Reconstructions after 10, 20 and 40 iterations for the full data case without added noise.

**Exact data:** Figure 3 shows the residuals and the relative  $L^2$ -reconstruction errors  $\|\mathbf{f}_k - \mathbf{f}\|_2 / \|\mathbf{f}\|_2$  of the above methods for the first 40 iterates applied to simulated data. For comparison purpose, we also show results using the TV minimization algorithm with  $\lambda = 0.1$ . One observes that the error and the residuals stagnate for all methods at some positive value after a certain number of iteration. This is because the minimizer of  $\|\mathbf{W}\mathbf{f} - \mathbf{g}^\delta\|_2^2$  is slightly different from the exact solution  $\mathbf{f}$  (since  $\mathbf{g} \neq \mathbf{g}^\delta$ , mainly due to the different data generation meshes). The CG method is the fastest converging and the Landweber the slowest. In Figure 4, we show reconstructions of these methods after 10, 20 and 40 iterations. All iterative methods have a similar behavior. In the initial iterations there are still artifacts contained in the pictures, and in later iterations the region with high attenuation value is underestimated. After more iterations, also this region is recovered correctly as well. The minimal reconstruction error  $\|\mathbf{f}_k - \mathbf{f}\|_2 / \|\mathbf{f}\|_2$  is about 2.9% and the minimal relative residual  $\|\mathbf{W}\mathbf{f}_k - \mathbf{g}\|_2 / \|\mathbf{g}\|_2$  about 3.5% for all methods.

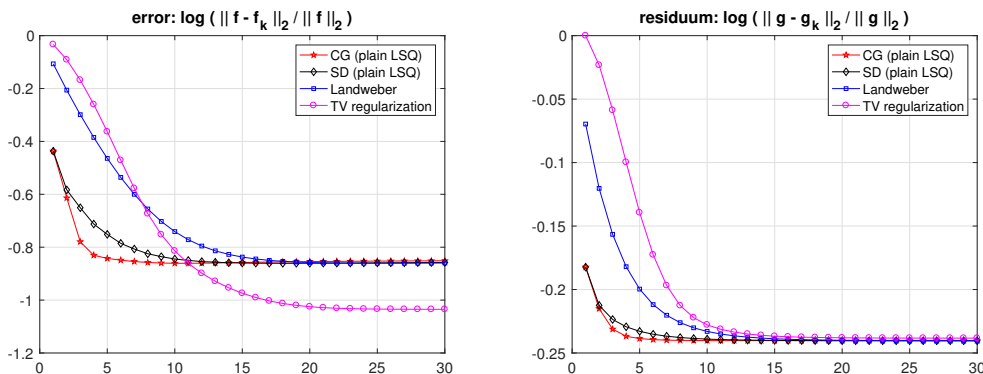


Figure 5: Errors and residuals for the full data case with noise added.

**Noisy data:** In order to test stability with respect to noise we repeated the above simulations after adding uniformly distributed Gaussian noise to the data with a relative error of about 59%. As can be seen from Figure 5, the convergence behavior is very similar to the exact data case reflecting the well-posedness of the inverse problem. Due to the added noise, the minimal residuals and the minimal reconstruction errors are of course much larger than in exact data case. Reconstructions after 5, 10 and 20 iterations are shown in Figure 6. One observes good reconstruction results and robustness with respect to the noise. The relative reconstruction errors after 20 iterations are about 14%, 13.8%, 13.9%, 9.4% for CG, steepest decent, Landweber and TV minimization, respectively. The relative residuals are 57.5%, 57.5%, 57.6%, 57.88% which is about the relative data error. One notes that the relative reconstruction error is even smaller than the relative data error. This is probably due to the redundancy of the PAT data. We conclude that in the full data case all methods have similar stability and accuracy, but the CG is the fastest. Therefore in the case of full data we can suggest the CG method among the unpenalized iterative methods for image reconstruction. In the case of the piecewise constant phantoms TV minimization seems to give better results in terms of  $L^2$ -reconstruction error.

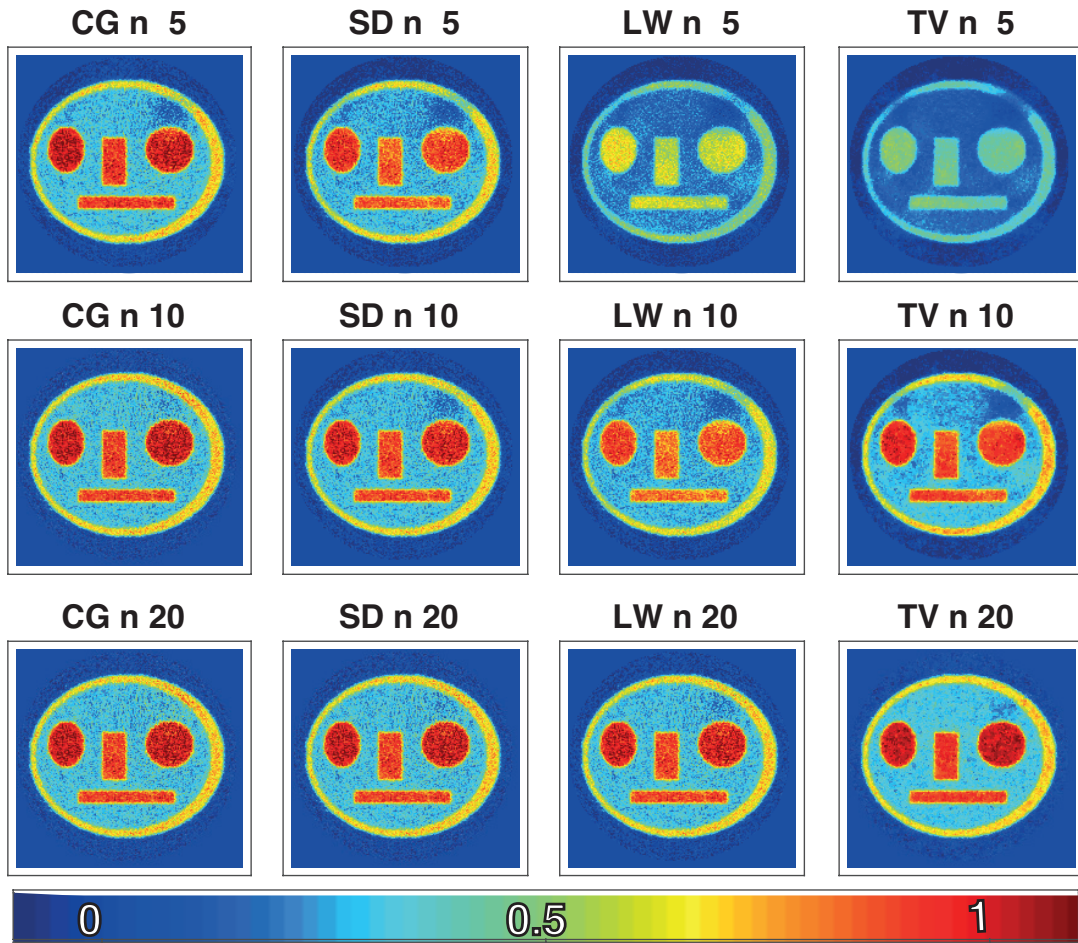


Figure 6: Reconstructions after 5, 10 and 20 iterations for the full data case with noise added.

#### 4.2 Limited view data (ill-posed case)

Next we consider the limited data where the data are only given on the part of the boundary  $\partial[-1, 1]^2$  determined by horizontal component being greater than  $-0.25$ . The visibility condition is not satisfied and we are facing a severely ill-posed problem for which one requires a regularization method. We propose the steepest descent and CG method as iterative regularization methods and  $H^1$ -regularization and TV-regularization as variational regularization methods. For minimizing the  $H^1$ -functional (8) we use the steepest descent iteration which, in our simulations, turned out to be faster than the Landweber method and more stable than the CG algorithm. For minimizing the TV-functional (9) we use the minimization algorithm of [49]. The regularization parameter in the variational methods is set to  $\lambda = 0.1$ .

**Exact data:** We start by applying the above schemes to the simulated data. Figure 7 shows the relative errors and relative residuals for all methods on a logarithmic scale.

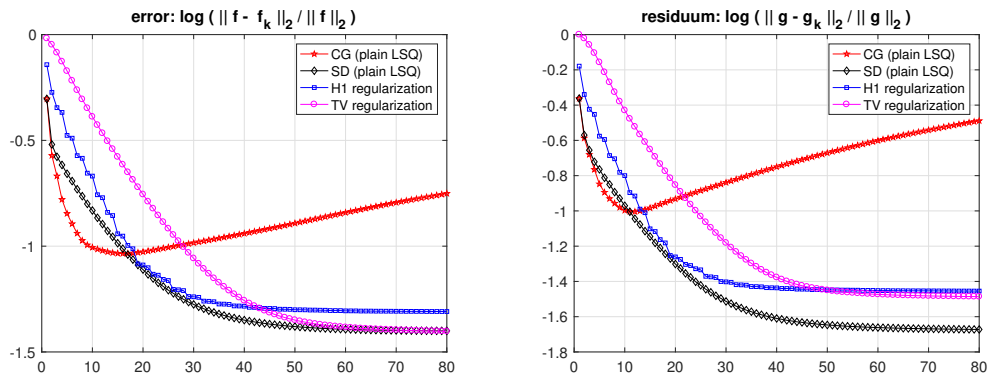


Figure 7: Errors and residuals for the ill-posed partial data case without noise.

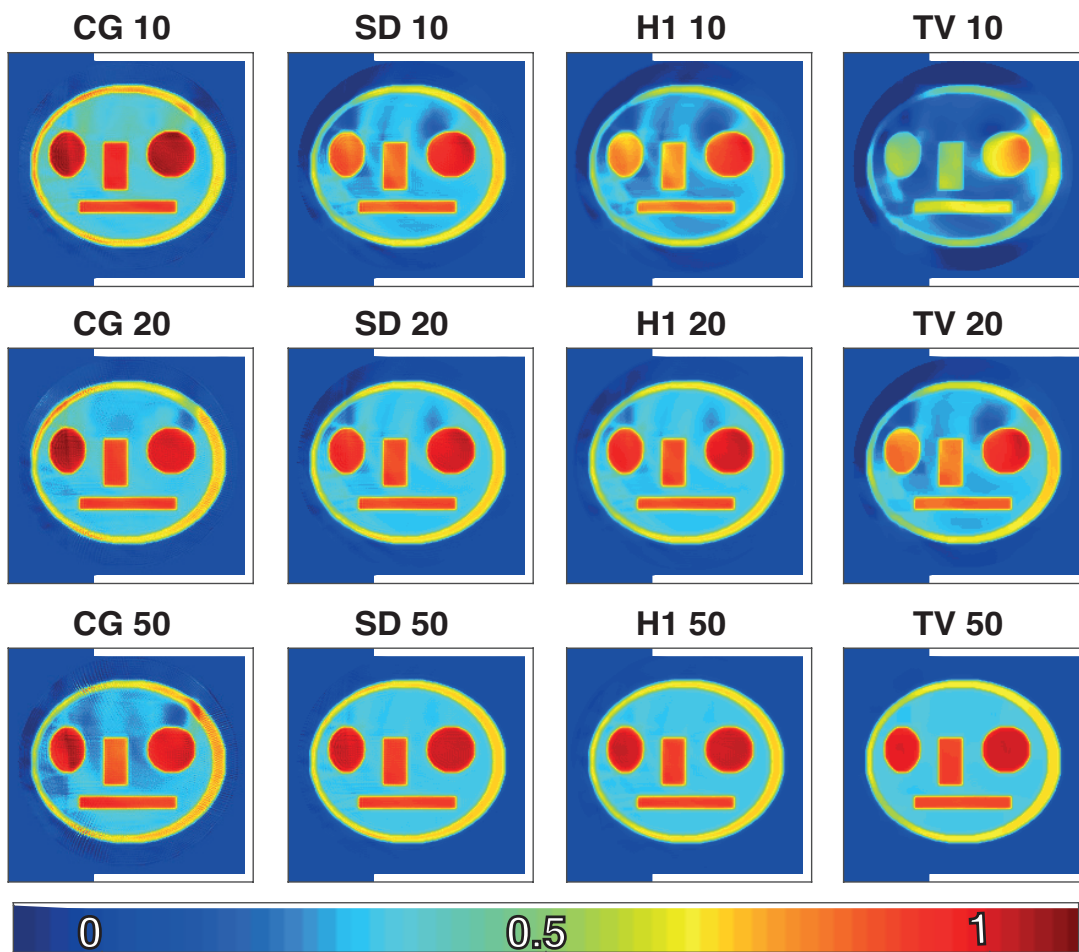


Figure 8: Reconstructions after 10, 20 and 50 iterations for the ill-posed partial data case without noise.

In terms of relative reconstruction errors, the steepest descent and the TV algorithm perform best, whereby the steepest descent is faster converging. Surprisingly, while



the CG method again shows very rapid convergence in the initial iterations, it turns out to be unstable in the ill-posed case. Reconstruction results after 10, 20 and 50 iterations are shown in the Figure 8. The relative  $\ell^2$ -reconstruction error after 50 iterations for the CG iteration, the steepest descent iteration,  $H^1$ -regularization and TV-regularization are 12.8%, 4.2%, 5%, and 4.5%, respectively. The corresponding (relative) residuals are 21.3%, 2.3%, 3.6%, and 3.6%.

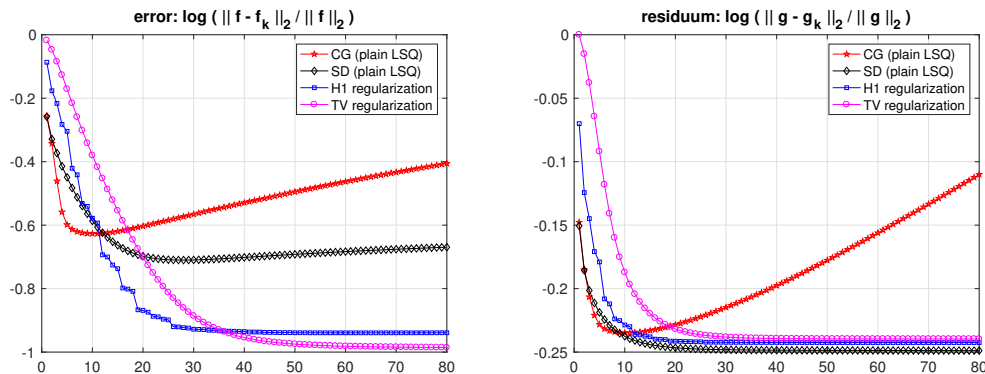


Figure 9: Errors and residuals for the ill-posed partial data case with noise.

**Noisy data:** The methods from above are again applied, now to noisy data with relative  $\ell^2$ -error about 59.7%. The standard (unpenalized) iterative methods provide a regularization method when combined with early stopping. In contrast, the  $H^1$ - and TV-regularization methods converge to the minimizers of the corresponding Tikhonov functionals. Reconstruction results are shown in Figures 9 and 10. In terms of reconstruction quality, TV-minimization is the best method, followed by  $H^1$ -regularization. The CG methods again behaves unstably and worse than the steepest descent method.

The relative  $\ell^2$ -reconstruction error after 50 iterations for the CG iteration, the steepest descent iteration,  $H^1$ -regularization and TV-regularization are respectively 32%, 20.3%, 11.5%, and 10.59%. The corresponding residuals are 66.4%, 56.4%, 57.2%, and 57.6%.

## Acknowledgements

Linh Nguyen's research is partially supported by the NSF grants DMS 1212125 and DMS 1616904. Markus Haltmeier acknowledges support of the Austrian Science Fund (FWF), project P 30747-N32.

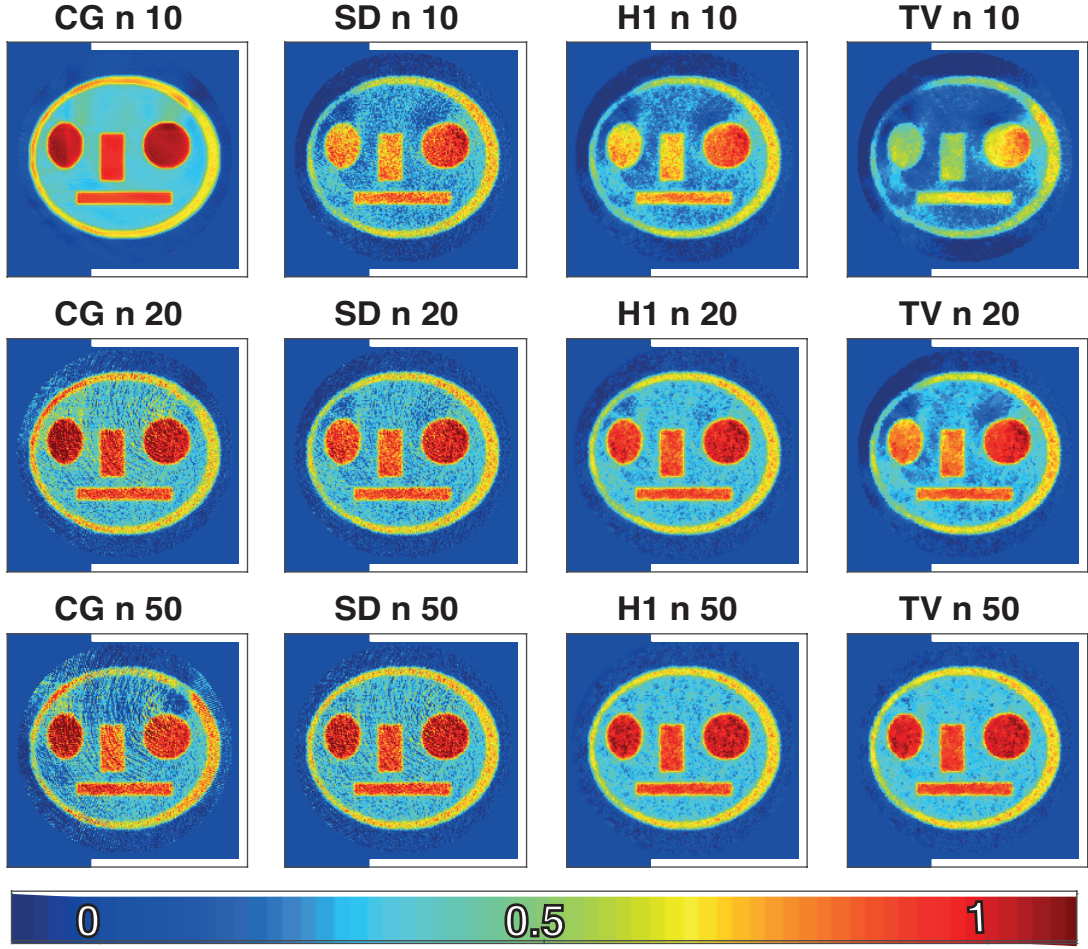


Figure 10: Reconstructions after 10, 20 and 50 iterations for the ill-posed partial data case with noise.

## A Appendix

### A.1 Existence and uniqueness of adjoint equation

In this section, we prove the existence and uniqueness for the adjoint equation. Namely, consider the equation:

$$\begin{cases} [c^{-2} \partial_{tt} + a \partial_t - \Delta]q = 0, & \text{for } (x, t) \in (\mathbb{R}^d \setminus \partial\Omega) \times (0, T), \\ q(0) = 0, \quad q_t(0) = 0, \\ [q] = 0, \quad \left[\frac{\partial q}{\partial \nu}\right] = g. \end{cases} \quad (10)$$

**Definition 7.** A function  $q$  is a weak solution of (10) if

$$\text{i) } q \in L^2([0, T]; H^1(\mathbb{R}^d)), \quad q' \in L^2([0, T]; L^2(\mathbb{R}^d)), \quad q'' \in L^2([0, T]; H^{-1}(\mathbb{R}^d)),$$



ii)  $q(0) = 0$  and  $q_t(0) = 0$ , and

iii) for any function  $\phi \in H_0^1(\mathbb{R}^d)$ :

$$\begin{aligned} \int_{\mathbb{R}^d} c^{-2}(x) q_{tt}(x, t) \phi(x) dx + \int_{\mathbb{R}^d} a(x) q_t(x, t) \phi(x) dx \\ + \int_{\mathbb{R}^d} \nabla q(x, t) \nabla \phi(x) dx = - \int_{\partial\Omega} g(y, t) \phi(y) dy, \quad \text{a.e. } t \in [0, T]. \end{aligned}$$

Let us note that from the above variational formulation, (10) can be formally rewritten as the nonhomogeneous wave problem

$$\begin{cases} [c^{-2} \partial_{tt} - a \partial_t - \Delta]q = -\delta_{\partial\Omega} g, & \text{on } \mathbb{R}^d \times (0, T), \\ q(0) = 0, \quad q_t(0) = 0, & \text{on } \mathbb{R}^d. \end{cases}$$

This formulation will be used for numerical simulation in Section A.2. Here are some results for equation (10):

**Theorem 8.** *For any*

$$g \in L^2([0, T]; H^{1/2}(\partial\Omega)) \cap H^1([0, T]; H^{-1/2}(\partial\Omega)),$$

*equation (10) has a unique weak solution. Moreover,*

- i)  $q$  satisfies the finite speed of propagation property. Namely, let  $c_+ := \max_{x \in \mathbb{R}^d} c(x)$ , then  $q(x, t) = 0$  for any  $(x, t) \in \Omega^c \times [0, T]$  such that  $\text{dist}(x, \partial\Omega) \geq c_+ t$ .
- ii) The following estimate holds

$$\int_0^T [\|q_t(t)\|^2 + \|q(t)\|_{H^1(\mathbb{R}^d)}^2] dt \leq C \|g'\|_{H^1([0, T]; H^{-1/2}(\partial\Omega))}^2. \quad (11)$$

Here, for simplicity, we use  $\|\cdot\|$  for the weighted  $L^2$ -norm with the weight  $c^{-2}(x)$ :

$$\|q_t(t)\|^2 = \int_{\mathbb{R}^d} c^{-2}(x) q_t^2(x, t) dx.$$

*Proof.* Let  $B_R$  denote the ball of radius  $R$  centered at the origin and  $R := R_0 + c_+ T$ , where  $R_0$  satisfies  $\Omega \subset B_{R_0}$ . Let  $H_0^1(B_R)$  be the closure of  $C_0^\infty(B_R)$  with respect to the norm

$$\|f\|_{H_0^1(B_R)} = \left[ \int_{B_R} |\nabla f|^2 dx \right]^{1/2}.$$

Our proof is divided into two steps:

*Step 1:* There exists a weak solution  $q$  of (10) on  $B_R$ . That is,

- i')  $q \in L^2([0, T]; H_0^1(B_R))$ ,  $q' \in L^2([0, T]; L^2(B_R))$ ,  $q'' \in L^2([0, T]; H^{-1}(B_R))$ ,
- ii')  $q(0) = 0$  and  $q'(0) = 0$ , and

iii') for any function  $\phi \in H_0^1(B_R)$

$$\begin{aligned} \int_{B_R} c^{-2}(x) q_{tt}(x, t) \phi(x) dx + \int_{B_R} a(x) q_t(x, t) \phi(x) dx \\ + \int_{B_R} \nabla q(x, t) \nabla \phi(x) dx = - \int_{\partial\Omega} g(y, t) \phi(y) dy \quad \text{a.e } t \in [0, T] \end{aligned}$$

*Step 2:* The solution  $q$  in Step 1 satisfies:  $q(x, t) = 0$  for all  $(x, t) \in \Omega^c \times [0, T]$  such that  $\text{dist}(x, \partial\Omega) \geq c_+ t$ .

Once both steps are proved, the solution  $q$  of equation (10) is just the trivial extension of  $q$  into  $[0, T] \times \mathbb{R}^d$ . Let us now proceed to prove those steps.

*Proof of Step 1:* Let  $\{\phi_k\}_k$  be an orthogonal basis of  $H_0^1(B_R)$ .<sup>1</sup> For any integer  $N$ , we define

$$q_N(x, t) = \sum_{i=1}^N d_i(t) \phi_i(x)$$

to be a solution of the system

$$\begin{aligned} \int_{B_R} c^{-2}(x) q_{N,tt}(x, t) \phi_i(x) dx + \int_{B_R} a(x) q_{N,t}(x, t) \phi_i(x) dx \\ + \int_{B_R} \nabla q_N(x, t) \nabla \phi_i(x) dx = - \int_{\partial\Omega} g(y, t) \phi_i(y) dy, \quad i = 1, \dots, N. \end{aligned} \quad (12)$$

together with the initial condition  $q_N(x, 0) = q_{N,t}(x, 0) = 0$ . Since the above system is a standard linear ODE system for  $(d_1, \dots, d_N)$ ,  $q_N$  uniquely exists. Multiplying each equation by  $d_i'(t)$  and summing them up, we obtain:

$$\begin{aligned} \int_{B_R} c^{-2}(x) q_{N,tt}(x, t) q_{N,t}(x, t) dx + \int_{B_R} a(x) [q_{N,t}(x, t)]^2 dx \\ + \int_{B_R} \nabla q_N(x, t) \nabla q_{N,t} dx = - \int_{\partial\Omega} g(y, t) q_{N,t}(y, t) dy. \end{aligned}$$

This implies

$$\frac{1}{2} \frac{d}{dt} \left[ \int_{B_R} c^{-2}(x) |q_{N,t}(x, t)|^2 dx + \int_{B_R} |\nabla q_N(x, t)|^2 dx \right] \leq - \int_{\partial\Omega} g(y, t) q_{N,t}(y, t) dy.$$

Taking the integration of both sides with respect to  $t$  and using the initial conditions for  $q_N$ :

$$\begin{aligned} \frac{1}{2} \left[ \|q_{N,t}(\cdot, t)\|^2 + \|q_N(\cdot, t)\|_{H_0^1(B_R)}^2 \right] \leq \\ - \int_{\partial\Omega} g(y, t) q_N(y, t) dy + \int_0^t \int_{\partial\Omega} g_t(y, t) q_N(y, t) dy. \end{aligned}$$

Bounding the first term of the right hand side, we obtain

$$\begin{aligned} \frac{1}{2} \left[ \|q_{N,t}(\cdot, t)\|^2 + \|q_N(\cdot, t)\|_{H_0^1(B_R)}^2 \right] \leq \|g(\cdot, t)\|_{H^{-1/2}(\partial\Omega)} \|q_N(\cdot, t)\|_{H^{1/2}(\partial\Omega)} \\ + \int_0^t \|g_t(\cdot, t)\|_{H^{-1/2}(\partial\Omega)}^2 + \int_0^t \|q_N(\cdot, t)\|_{H^{1/2}(\partial\Omega)}. \end{aligned}$$

---

<sup>1</sup>One such basis is the set of normalized eigenvectors of the Laplacian with the zero boundary condition.

Now, Young's inequality gives

$$\begin{aligned} \frac{1}{2} \left[ \|q_{N,t}(\cdot, t)\|^2 + \|q_N(\cdot, t)\|_{H_0^1(B_R)}^2 \right] &\leq A \|g(\cdot, t)\|_{H^{-1/2}(\partial\Omega)}^2 \\ &+ \frac{1}{2A} \|q_N(\cdot, t)\|_{H^{1/2}(\partial\Omega)}^2 + \int_0^t \|g_t(\cdot, t)\|_{H^{-1/2}(\partial\Omega)}^2 + \int_0^t \|q_N(\cdot, t)\|_{H^{1/2}(\partial\Omega)}, \end{aligned}$$

where  $A > 0$  can be any constant, whose value will be specified later. Noting that  $\|q_N(\cdot, t)\|_{H^{1/2}(\partial\Omega)} \leq C \|q_N(\cdot, t)\|_{H_0^1(B_R)}$  we obtain by choosing  $A$  big enough

$$\begin{aligned} \frac{1}{2} \left[ \|q_{N,t}(\cdot, t)\|^2 + \|q_N(\cdot, t)\|_{H_0^1(B_R)}^2 \right] &\leq A \|g(\cdot, t)\|_{H^{-1/2}(\partial\Omega)}^2 \\ &+ \frac{1}{4} \|q_N(\cdot, t)\|_{H_0^1(B_R)}^2 + \int_0^t \|g_t(\cdot, t)\|_{H^{-1/2}(\partial\Omega)}^2 + C \int_0^t \|q_N(\cdot, t)\|_{H_0^1(B_R)}^2. \end{aligned}$$

Here and in the sequel,  $C$  is a generic constant whose value may vary from one place to another. Therefore,

$$\begin{aligned} \|q_{N,t}(\cdot, t)\|^2 + \|q_N(\cdot, t)\|_{H_0^1(B_R)}^2 &\leq C (\|g(\cdot, t)\|_{H^{-1/2}(\partial\Omega)}^2 \\ &+ \int_0^t \|g_t(\cdot, t)\|_{H^{-1/2}(\partial\Omega)}^2 + \int_0^t \|q_N(\cdot, t)\|_{H_0^1(B_R)}^2), \quad t \in [0, T]. \end{aligned}$$

Let  $E_N(t) := \int_0^t \|q_{N,t}(\cdot, t)\|^2 + \|q_N(\cdot, t)\|_{H^1(B_R)}^2$ . We arrive at

$$E'_N(t) - CE_N(t) \leq C (\|g(\cdot, t)\|_{H^{-1/2}(\partial\Omega)}^2 + \|g_t\|_{L^2([0,T], H^{-1/2}(\partial\Omega))}^2), \quad t \in [0, T].$$

From the Grownwall's inequality, we obtain

$$E_N(T) \leq C (\|g\|_{L^2([0,T], H^{-1/2}(\partial\Omega))}^2 + \|g_t\|_{L^2([0,T], H^{-1/2}(\partial\Omega))}^2). \quad (13)$$

Since  $C$  is a constant independent of  $N$ ,  $\{q_N\}$  and  $\{q_{N,t}\}$  are bounded sequences in  $L^2([0, T], H_0^1(B_R))$  and  $L^2([0, T]; L^2(B_R))$ , respectively. After possibly passing over to subsequences, we obtain  $q_N \rightharpoonup q$  in  $L^2([0, T]; H_0^1(B_R))$  and  $q_{N,t} \rightharpoonup q_t$  in  $L^2([0, T]; L^2(B_R))$ . It is easy to show that  $q_1 = q'$ . Since  $\{\phi_k\}$  is a basis of  $H_0^1(B_R)$ , from (12), we obtain for any  $v \in L^2([0, T]; H_0^1(\Omega))$ :

$$\begin{aligned} \lim_{N \rightarrow \infty} \int_0^T \int_{\mathbb{R}^d} c^{-2}(x) q_{N,tt}(x, t) v(x, t) dx dt + \int_0^T \int_{\mathbb{R}^d} a(x) q_t(x, t) v(x, t) dx dt \\ + \int_0^T \int_{\mathbb{R}^d} \nabla q(x, t) \nabla v(x, t) dx = - \int_{\partial\Omega} g(y, t) v(y, t) dy. \end{aligned}$$

That is,  $q_{N,tt}$  converges to an element in  $L^2([0, T], H^{-1}(B_R))$ . That is,  $q_{tt} \in L^2([0, T], H^{-1}(B_R))$  and

$$\begin{aligned} \int_0^T \int_{\mathbb{R}^d} c^{-2}(x) q_{tt}(x, t) v(x, t) dx dt + \int_0^T \int_{\mathbb{R}^d} a(x) q_t(x, t) v(x, t) dx dt \\ + \int_0^T \int_{\mathbb{R}^d} \nabla q(x, t) \nabla v(x, t) dx dt = - \int_0^T \int_{\partial\Omega} g(y, t) v(y, t) dy dt. \end{aligned}$$

Let  $\phi \in H_0^1(B_R)$ . For any  $t_0 \in (0, T)$ , choosing<sup>2</sup>  $v(x, t) = \phi(x)\chi_{[t_0-\epsilon, t_0+\epsilon]}(t)$ , we obtain

$$\begin{aligned} & \int_{t_0-\epsilon}^{t_0+\epsilon} \int_{\mathbb{R}^d} c^{-2}(x) q_{tt}(x, t) \phi(x) dx dt + \int_{t_0-\epsilon}^{t_0+\epsilon} \int_{\mathbb{R}^d} a(x) q_t(x, t) \phi(x) dx dt \\ & \quad + \int_{t_0-\epsilon}^{t_0+\epsilon} \int_{\mathbb{R}^d} \nabla q(x, t) \nabla \phi(x) dx dt = - \int_{t_0-\epsilon}^{t_0+\epsilon} \int_{\partial\Omega} g(y, t) \phi(y) dy dt. \end{aligned}$$

Dividing both sides by  $2\epsilon$  and send  $\epsilon \rightarrow 0$ , we obtain

$$\begin{aligned} & \int_{B_R} c^{-2}(x) q_{tt}(x, t_0) \phi(x) dx + \int_{B_R} a(x) q_t(x, t_0) \phi(x) dx \\ & \quad + \int_{B_R} \nabla q(x, t_0) \nabla \phi(x) dx = - \int_{\partial\Omega} g(y, t_0) \phi(y) dy \quad \text{a.e } t_0 \in [0, T] \end{aligned}$$

This finishes the proof of Step 1, since ii') easily follows from the fact that  $q_N(\cdot, 0) = 0$  and  $q_{N,t}(\cdot, 0) = 0$ .

*Proof of step 2:* We first prove the result in the case  $u' \in L^2([0, T], H^1(\Omega))$  and  $u'' \in L^2([0, T], L^2(\Omega))$ . Let  $(x_0, t_0) \in (B_R \setminus \Omega) \times [0, T]$  such that  $\text{dist}(x_0, \partial\Omega) > c_+ t_0$ . There is  $\epsilon_0 > 0$  such that for each  $t \in [0, t_0]$ , we have  $B(x_0, (c_+ + \epsilon_0)(t_0 - t)) \cap \partial\Omega = \emptyset$ . We also denote  $\mathcal{O}_t = B(x_0, c(t_0 - t)) \cap B_R$  and

$$E(t) = \frac{1}{2} \int_{\mathcal{O}_t} c^{-2}(x) |q_t(x, t)|^2 + |\nabla q(x, t)|^2 dx, \quad 0 \leq t \leq t_0.$$

Then,

$$\begin{aligned} \frac{d}{dt} E(t) &= -\frac{c_+}{2} \int_{\partial\mathcal{O}_t \setminus \partial B_R} c^{-2}(x) |q_t(x, t)|^2 + |\nabla q(x, t)|^2 d\sigma(x) \\ & \quad + \int_{\mathcal{O}_t} c^{-2}(x) q_t(x, t) q_{tt}(x, t) + \nabla q(x, t) \nabla q_t(x, t) dx. \end{aligned}$$

Taking integration by parts for the second integral gives the following formula of  $\frac{d}{dt} E(t)$ :

$$\begin{aligned} & -\frac{c_+}{2} \int_{\partial\mathcal{O}_t \setminus \partial\Omega_R} [c^{-2}(x) |q_t(x, t)|^2 + |\nabla q(x, t)|^2 - 2\partial_\nu q(x, t) \\ & \quad \times \frac{q_t(x, t)}{c_+}] d\sigma(x) + \int_{\mathcal{O}_t} [c^{-2}(x) q_{tt}(x, t) - \Delta q(x, t)] q_t(x, t) dx. \end{aligned}$$

Noting that the integrand of the first term on the right hand side is nonnegative, we arrive to

$$\frac{d}{dt} E(t) \leq \int_{\mathcal{O}_t} [c^{-2}(x) q_{tt}(x, t) - \Delta q(x, t)] q_t(x, t) dx.$$

Let us recall that for any function  $\phi \in H_0^1(B_R)$

$$\begin{aligned} & \int_{B_R} c^{-2}(x) q_{tt}(x, t) \phi(x) dx + \int_{B_R} a(x) q_t(x, t) \phi(x) dx \\ & \quad + \int_{B_R} \nabla q(x, t) \nabla \phi(x) dx = - \int_{\partial\Omega} g(y, t) \phi(x) dy. \end{aligned}$$

---

<sup>2</sup>For any set  $U$ ,  $\chi_U$  is the characteristic function of  $U$ .

For  $0 < \epsilon < \epsilon_0$  we choose  $\varphi_\epsilon \in C^\infty(\mathbb{R}^d)$  be a nonnegative function such that  $\varphi \equiv 1$  on  $B_{(x_0, c_+(t_0-t))}$  and  $\varphi \equiv 0$  outside of  $B_{(x_0, (c_++\epsilon)(t_0-t))}$  and  $\lim_{\epsilon \rightarrow 0} \varphi_\epsilon = \chi_{B_{x_0, c_+(t_0-t)}}$  on  $L^2(\mathbb{R}^d)$ . Choosing  $\phi(x) = q_t(x, t)\varphi_\epsilon(x)$ , we obtain

$$\begin{aligned} \int_{B_R} c^{-2}(x) q_{tt}(x, t) q_t(x, t) \varphi_\epsilon(x) dx + \int_{B_R} a(x) q_t(x, t) q_t(x, t) \varphi_\epsilon(x) dx \\ + \int_{B_R} \nabla q(x, t) \nabla [v_t(x, t) \varphi_\epsilon(x)] dx = 0. \end{aligned}$$

Taking integration by parts for the last integral and combine it with the first integral, we obtain

$$\int_{B_R} \left[ c^{-2}(x) q_{tt}(x, t) - \Delta q(x, t) \right] q_t(x, t) \varphi_\epsilon(x) dx + \int_{B_R} a(x) q_t^2(x, t) \varphi_\epsilon(x) dx = 0.$$

Therefore,

$$\int_{B_R} \left[ c^{-2}(x) q_{tt}(x, t) - \Delta q(x, t) \right] q_t(x, t) \varphi_\epsilon(x) dx \leq 0.$$

Taking the limit as  $\epsilon \rightarrow 0$ , we obtain

$$\int_{\mathcal{O}_t} \left[ c^{-2}(x) q_{tt}(x, t) - \Delta q(x, t) \right] q_t(x, t) dx \leq 0.$$

We obtain  $\frac{E(t)}{dt} \leq 0$ . Noting that  $E(0) = 0$ , we arrive at  $E(t) = 0$  for all  $t \in [0, t_0]$ . Therefore,  $q(x, t) = 0$  on  $\mathcal{O}_t$  for all  $t \in [0, t_0]$ . Since this is correct for all  $(x_0, t_0) \in \Omega^c \times [0, T]$  such that  $\text{dist}(x_0, \partial\Omega) > c_+ t_0$ , It is now easy to see  $q(x, t) = 0$  for all  $(x, t) \in \Omega^c$  such that  $\text{dist}(x, \partial\Omega) \geq c_+ t$ .

In general, we do not have the required regularity for the above proof. However, consider  $Q(x, t) = \int_0^t q(x, \tau) d\tau$ . Then,  $Q$  satisfies the same equation (with a different jump function) and the required regularity. The above proof then shows that  $Q(x, t) = 0$  for all  $(x, t) \in \Omega^c \times [0, T]$  such that  $\text{dist}(x, \partial\Omega) \geq c_+ t$ . It implies the same result for  $q(x, t)$ . This finishes proof of Step 2.

*Finishing the proof:* Now extending  $q$  into  $\mathbb{R}^d \times [0, T]$  by zero on  $(\mathbb{R}^d \setminus B_R) \times [0, T]$ , we can easily prove that  $q$  is a weak solution on  $\mathbb{R}^d \times [0, T]$ . Moreover,  $q$  satisfies the finite speed of propagation (i). Finally, the estimate (11) follows from (13). The uniqueness of  $q$  is simple (see, e.g., proof of Theorem A.2 in [8]), we leave the details to the reader.  $\square$

## A.2 A $k$ -space method for the damped wave equation

In this subsection, we briefly describe the  $k$ -space method as we use it to numerically compute the solution of the wave equation, which is required for evaluating the forward operator  $\mathbf{W}$  and its adjoint  $\mathbf{W}^*$ . For the case  $a = 0$ , several methods for numerically solving the underlying acoustic wave equation have been used in PAT. This includes finite difference methods [10, 41, 52], finite element methods [8] as well as Fourier spectral and  $k$ -space methods [14, 27, 54]. We now extend the  $k$ -space method to the case  $a \neq 0$  because this method does not suffer from numerical dispersion [13].

Consider the solution  $p: \mathbb{R}^d \times (0, T) \rightarrow \mathbb{R}$  of the damped wave equation

$$[c^{-2} \partial_{tt} + a \partial_t - \Delta]p = s \quad \text{on } \mathbb{R}^d \times (0, T), \quad (14)$$

$$p(0) = f \quad \text{on } \mathbb{R}^d, \quad (15)$$

$$p_t(0) = -c^2 a f \quad \text{on } \mathbb{R}^d. \quad (16)$$

Here,  $s: \mathbb{R}^d \times (0, T) \rightarrow \mathbb{R}$  is a given source term and  $f: \mathbb{R}^d \rightarrow \mathbb{R}$  the given initial pressure. To derive the  $k$ -space method one first rewrites (14) in the form

$$[\partial_{tt} - c_0^2 \Delta]p = (1 - c_0^2/c^2)p_{tt} - c_0^2 a p_t + c_0^2 s \quad (17)$$

where  $c_0 > 0$  is a suitable constant; we take  $c_0 = c_+ := \max\{c(x) : x \in \mathbb{R}^2\}$ .

The  $k$ -space method is derived from (17) by introducing the auxiliary functions  $v(x, t)$  and  $r(x, t)$  such that  $v_{tt}(x, t) = (1 - c_0^2/c^2(x))p_{tt}(x, t)$  and  $r_{tt}(x, t) = c_0^2 a(x)p_t(x, t)$ . Such an approach shows that (17) is equivalent to the following system of equations,

$$[\partial_{tt} - c_0^2 \Delta]w = c_0^2 s + c_0^2 \Delta v - c_0^2 \Delta r, \quad (18)$$

$$v = (c^2/c_0^2 - 1)(w - r) \quad (19)$$

$$p = v + w - r \quad (20)$$

$$r(t) = c_0^2 a \int_0^t p(s) ds. \quad (21)$$

Interpreting  $c_0^2 \Delta v(x, t) - c_0^2 \Delta r(x, t)$  as an additional source term, (18) is a standard wave equation with constant sound speed  $c_0$ . This suggests the time stepping formula

$$w(x, t + h_t) = 2w(x, t) - w(x, t - h_t) - 4\mathcal{F}_\xi^{-1} \left[ \sin(c_0 |\xi| h_t/2)^2 \times \right. \\ \left. \mathcal{F}_x [w(x, t) + v(x, t) - r(x, t)] - (c_0 h_t/2)^2 \text{sinc}(c_0 |\xi| h_t/2)^2 \mathcal{F}_x [s(x, t)] \right], \quad (22)$$

where  $\mathcal{F}_x$  and  $\mathcal{F}_\xi^{-1}$  denote the Fourier and inverse Fourier transforms in the spatial variable  $x$  and the spatial frequency variable  $\xi$ , respectively, and  $h_t > 0$  is a time stepping size.

The resulting  $k$ -space method for solving (14) is summarized in Algorithm 1.

**Algorithm 1** (The  $k$ -space method). For given initial pressure  $f(x)$  and source term  $s(x, t)$  approximate the solution  $p(x, t)$  of (14) as follows:

(1) Set  $t = 0$  and define initial conditions

- $r(x, 0) = 0$ ;
- $v(x, 0) = (1 - c_0^2/c^2(x))f(x)$ ;
- $w(x, 0) = c_0^2/c^2(x)f(x)$ ;
- $w(x, -h_t) = (1 + h_t c_0^2 a(x))w(x, 0)$ .

(2) Compute  $w(x, t + h_t)$  by evaluating (22);

(3) Make the updates

- $v(x, t + h_t) := (c^2(x)/c_0^2 - 1) (w(x, t + h_t) - r(x, t));$
- $p(x, t + h_t) := v(x, t + h_t) + w(x, t + h_t) - r(x, t);$
- $r(x, t + h_t) := r(x, t) + c_0^2 a(x) p(x, t + h_t) h_t;$

(4) Set  $t \leftarrow t + h_t$  and go back to (3).

Algorithm 1 can directly be used to evaluate the forward operator  $\mathbf{W}f$  by taking  $s(x, t) = 0$  and restricting the solution to the measurement surface  $S_R$ , that is  $\mathbf{W}f = p|_{S_R \times (0, T)}$ . Recall that the adjoint operator is given by  $\mathbf{W}^*g = q_t(0)$ , where  $q: \mathbb{R}^2 \times (0, T) \rightarrow \mathbb{R}$  satisfies the adjoint wave equation

$$[c^{-2} \partial_{tt} - \Delta]q = -\delta_{S_R} g \quad \text{on } \mathbb{R}^2 \times (0, T) \quad (23)$$

$$q_t(T) = q(T) = 0 \quad \text{on } \mathbb{R}^d. \quad (24)$$

By substituting  $t \leftarrow T - t$  and taking  $s(x, t) = g(x, T - t) \delta_S(x)$  as source term in 14, Algorithm 1 can also be used to evaluate the  $\mathbf{W}^*$ . In the partial data case where measurements are made on a subset  $S \subsetneq S_R$  only, the adjoint can be implemented by taking the source  $s(x, t) = \chi(x, t) g(x, T - t) \delta_{S_R}(x)$  with an appropriate window function  $\chi(x, t)$ . In order to use all available data, in our implementations we take the window function to be equal to one on the observation part  $S$  and zero outside. This choice of the window function is known to create streak artifacts into the picture [19, 40, 7]. However, as we see in our simulations, the artifacts fade away quickly after several iterations when the problem is well-posed.

## References

- [1] S. Acosta and B. Palacios, Thermoacoustic tomography for an integro-differential wave equation modeling attenuation. arXiv:1703.09271 [math.AP], 2017.
- [2] M. Agranovsky and P. Kuchment, Uniqueness of reconstruction and an inversion procedure for thermoacoustic and photoacoustic tomography with variable sound speed, *Inverse Problems*, 23 (2007), p. 2089.
- [3] H. Ammari, E. Bretin, J. Garnier, and A. Wahab, Time reversal in attenuating acoustic media, *Contemporary Mathematics*, 548 (2011), pp. 151–163.
- [4] H. Ammari, E. Bretin, V. Jugnon, and A. Wahab, Photoacoustic imaging for attenuating acoustic media, in *Mathematical modeling in biomedical imaging II*, Springer, 2012, pp. 57–84.
- [5] S. Arridge, P. Beard, M. Betcke, B. Cox, N. Huynh, F. Lucka, O. Ogunlade, and E. Zhang, Accelerated high-resolution photoacoustic tomography via compressed sensing, *Phys. Med. Biol.*, 61 (2016), p. 8908.
- [6] S. R. Arridge, M. M. Betcke, B. T. Cox, F. Lucka, and B. E. Treeby, On the adjoint operator in photoacoustic tomography, *Inverse Problems*, 32 (2016), p. 115012 (19pp).

- [7] L. L. Barannyk, J. Frikel, and L. V. Nguyen, On Artifacts in Limited Data Spherical Radon Transform: Curved Observation Surface, *Inverse Problems*, 32 (2015).
- [8] Z. Belhachmi, T. Glatz, and O. Scherzer, A direct method for photoacoustic tomography with inhomogeneous sound speed, *Inverse Problems*, 32 (2016), p. 045005.
- [9] P. Burgholzer, H. Grün, M. Haltmeier, R. Nuster, and G. Paltauf, Compensation of acoustic attenuation for high-resolution photoacoustic imaging with line detectors, *Proceedings of SPIE*, vol. 6437 (2007), p. 643724.
- [10] P. Burgholzer, G. J. Matt, M. Haltmeier, and G. Paltauf, Exact and approximate imaging methods for photoacoustic tomography using an arbitrary detection surface, *Physical Review E*, 75 (2007), p. 046706.
- [11] A. Chambolle and T. Pock, A first-order primal-dual algorithm for convex problems with applications to imaging, *J. Math. Imaging Vision*, 40 (2011), pp. 120–145.
- [12] C. Clason and M. V. Klibanov, The quasi-reversibility method for thermoacoustic tomography in a heterogeneous medium, *SIAM Journal on Scientific Computing*, 30 (2008), pp. 1–23.
- [13] B. Compani-Tabrizi, K-space scattering formulation of the absorptive full fluid elastic scalar wave equation in the time domain, *The Journal of the Acoustical Society of America*, 79 (1986), pp. 901–905.
- [14] B. Cox, S. Kara, S. Arridge, and P. Beard, k-space propagation models for acoustically heterogeneous media: Application to biomedical photoacoustics, *The Journal of the Acoustical Society of America*, 121 (2007), pp. 3453–3464.
- [15] X. L. Dean-Ben, A. Buehler, V. Ntziachristos, and D. Razansky, Accurate model-based reconstruction algorithm for three-dimensional optoacoustic tomography, *IEEE Trans. Med. Imag.*, 31 (2012), pp. 1922–1928.
- [16] H. W. Engl, M. Hanke, and A. Neubauer, *Regularization of inverse problems*, vol. 375, Springer Science & Business Media, 1996.
- [17] D. Finch, M. Haltmeier, and Rakesh, Inversion of spherical means and the wave equation in even dimensions, *SIAM Journal on Applied Mathematics*, 68 (2007), pp. 392–412.
- [18] D. Finch, S. K. Patch, and Rakesh, Determining a function from its mean values over a family of spheres, *SIAM Journal on Mathematical Analysis*, 35 (2004), pp. 1213–1240 (electronic).
- [19] J. Frikel and E. T. Quinto, Artifacts in incomplete data tomography with applications to photoacoustic tomography and sonar, *SIAM Journal on Applied Mathematics*, 75 (2015), pp. 703–725.
- [20] M. Haltmeier, Inversion of circular means and the wave equation on convex planar domains, *Computers & Mathematics with Applications. An International Journal*, 65 (2013), pp. 1025–1036.



- [21] ———, Universal inversion formulas for recovering a function from spherical means, *SIAM Journal on Mathematical Analysis*, 46 (2014), pp. 214–232.
- [22] M. Haltmeier and L. V. Nguyen, Analysis of iterative methods in photoacoustic tomography with variable sound speed, *SIAM J. Imaging Sci.*, 10 (2017), pp. 751–781.
- [23] M. Hanke, *Conjugate gradient type methods for ill-posed problems*, vol. 327, CRC Press, 1995.
- [24] A. Homan, Multi-wave imaging in attenuating media, *Inverse Probl. Imaging*, 7 (2013), pp. 1235–1250.
- [25] Y. Hristova, Time reversal in thermoacoustic tomography—an error estimate, *Inverse Problems*, 25 (2009), pp. 055008, 14.
- [26] Y. Hristova, P. Kuchment, and L. Nguyen, Reconstruction and time reversal in thermoacoustic tomography in acoustically homogeneous and inhomogeneous media, *Inverse Problems*, 24 (2008), pp. 055006, 25.
- [27] C. Huang, K. Wang, L. Nie, and M. A. Wang, L. V. and Anastasio, Full-wave iterative image reconstruction in photoacoustic tomography with acoustically inhomogeneous media, *IEEE Trans. Med. Imag.*, 32 (2013), pp. 1097–1110.
- [28] A. Javaherian and S. Holman, A multi-grid iterative method for photoacoustic tomography, *IEEE Trans. Med. Imag.*, 36 (2017), pp. 696–706.
- [29] B. Kaltenbacher, A. Neubauer, and O. Scherzer, Iterative regularization methods for nonlinear ill-posed problems, vol. 6 of *Radon Series on Computational and Applied Mathematics*, Walter de Gruyter GmbH & Co. KG, Berlin, 2008.
- [30] R. Kowar, On time reversal in photoacoustic tomography for tissue similar to water, *SIAM J. Imaging Sci.*, 7 (2014), pp. 509–527.
- [31] R. Kowar and O. Scherzer, Photoacoustic imaging taking into account attenuation, in *Mathematics and Algorithms in Tomography*, vol. 18, Springer, 2012, pp. 54–56.
- [32] P. Kuchment, *The Radon transform and medical imaging*, vol. 85, SIAM, 2014.
- [33] P. Kuchment and L. Kunyansky, Mathematics of thermoacoustic tomography, *European Journal of Applied Mathematics*, 19 (2008), pp. 191–224.
- [34] L. A. Kunyansky, Explicit inversion formulae for the spherical mean Radon transform, *Inverse Problems*, 23 (2007), pp. 373–383.
- [35] L. A. Kunyansky, A series solution and a fast algorithm for the inversion of the spherical mean radon transform, *Inverse Problems*, 23 (2007), p. S11.
- [36] P. J. La Riviere, J. Zhang, and M. A. Anastasio, Image reconstruction in optoacoustic tomography accounting for frequency-dependent attenuation, *Nuclear Science Symposium Conference Record, 2005 IEEE*, 4 (2005), p. 5 pp.
- [37] P. J. La Rivière, J. Zhang, and M. A. Anastasio, Image reconstruction in optoacoustic tomography for dispersive acoustic media, *Opt. Lett.*, 31 (2006), pp. 781–783.

- [38] F. Natterer, Photo-acoustic inversion in convex domains, *Inverse Problems Imaging*, (2012).
- [39] L. V. Nguyen, A family of inversion formulas in thermoacoustic tomography, *Inverse Probl. Imaging*, 3 (2009), pp. 649–675.
- [40] L. V. Nguyen, On artifacts in limited data spherical radon transform: Flat observation surfaces, *SIAM J. Math. Analysis*, 47 (2015), pp. 2984–3004.
- [41] L. V. Nguyen and L. A. Kunyansky, A dissipative time reversal technique for photoacoustic tomography in a cavity, *SIAM Journal on Imaging Sciences*, 9 (2016), pp. 748–769.
- [42] B. Palacios, Reconstruction for multi-wave imaging in attenuating media with large damping coefficient, *Inverse Probl.*, 32 (2016), pp. 125008, 15.
- [43] V. P. Palamodov, A uniform reconstruction formula in integral geometry, *Inverse Probl.*, 28 (2012), p. 065014.
- [44] G. Paltauf, R. Nuster, M. Haltmeier, and P. Burgholzer, Experimental evaluation of reconstruction algorithms for limited view photoacoustic tomography with line detectors, *Inverse Probl.*, 23 (2007), pp. S81–S94.
- [45] G. Paltauf, J. A. Viator, S. A. Prahl, and S. L. Jacques, Iterative reconstruction algorithm for optoacoustic imaging, *J. Opt. Soc. Am.*, 112 (2002), pp. 1536–1544.
- [46] A. Rosenthal, V. Ntziachristos, and D. Razansky, Acoustic inversion in optoacoustic tomography: A review, *Current medical imaging reviews*, 9 (2013), p. 318.
- [47] ———, Acoustic inversion in optoacoustic tomography: A review, *Current medical imaging reviews*, 9 (2013), p. 318.
- [48] O. Scherzer, M. Grasmair, H. Grossauer, M. Haltmeier, and F. Lenzen, *Variational methods in imaging*, volume 167 of applied mathematical sciences, 2009.
- [49] E. Y. Sidky, J. H. Jørgensen, and X. Pan, Convex optimization problem prototyping for image reconstruction in computed tomography with the chambolle–pock algorithm, *Phys. Med. Biol.*, 57 (2012), p. 3065.
- [50] P. Stefanov and G. Uhlmann, Thermoacoustic tomography with variable sound speed, *Inverse Problems*, 25 (2009), pp. 075011, 16.
- [51] P. Stefanov and G. Uhlmann, Thermoacoustic tomography arising in brain imaging, *Inverse Problems*, 27 (2011), p. 045004.
- [52] P. Stefanov and Y. Yang, Multiwave tomography with reflectors: Landweber’s iteration, *ArXiv e-prints*, (2016).
- [53] M. E. Taylor, *Pseudodifferential operators*, volume 34 of princeton mathematical series, 1981.
- [54] B. E. Treeby and B. T. Cox, k-wave: Matlab toolbox for the simulation and reconstruction of photoacoustic wave fields, *Journal of biomedical optics*, 15 (2010), pp. 021314–021314.

- [55] B. E. Treeby, E. Z. Zhang, and B. Cox, Photoacoustic tomography in absorbing acoustic media using time reversal, *Inverse Probl.*, 26 (2010), p. 115003.
- [56] K. Wang, R. W. Schoonover, R. Su, A. Oraevsky, and M. A. Anastasio, Discrete imaging models for three-dimensional optoacoustic tomography using radially symmetric expansion functions, *IEEE Trans. Med. Imag.*, 33 (2014), pp. 1180–1193.
- [57] K. Wang, R. Su, A. A. Oraevsky, and M. A. Anastasio, Investigation of iterative image reconstruction in three-dimensional optoacoustic tomography, *Physics in medicine and biology*, 57 (2012), p. 5399.
- [58] M. Xu and L. V. Wang, Universal back-projection algorithm for photoacoustic computed tomography, *Physical Review E*, 71 (2005).
- [59] J. Zhang, M. A. Anastasio, P. J. La Rivière, and L. V. Wang, Effects of different imaging models on least-squares image reconstruction accuracy in photoacoustic tomography, *IEEE Trans. Med. Imag.*, 28 (2009), pp. 1781–1790.